Phase inhomogeneity and inapplicability of J_{eff}=0 description in dilute Ir^{5+} doped $Ba_2YSb_{1-x}Ir_xO_6$ ($x = 0.1, 0.2, 0.3$)

Md Salman Khan [1], Carlo Meneghini,[2] Fabrice Bert,[3] M. Moretti Sala [4,5] and Sugata Ray [1,6,*]

[1] *School of Materials Science, Indian Association for the Cultivation of Science, 2A & 2B Raja S. C. Mullick Road, Jadavpur, Kolkata 700032, India*

[2] *Dipartimento di Scienze, Universitá Roma Tre, Via della Vasca Navale, 84 I-00146 Roma, Italy*

[3] *Laboratoire de Physique des Solides, UMR CNRS 8502, Université Paris-Sud, 91405 Orsay, France*

[4] *ESRF The European Synchrotron, 71 Avenue des Martyrs, 38000 Grenoble, France*

[5] *Dipartimento di Fisica, Politecnico di Milano, P.zza Leonardo da Vinci 32, I-20133 Milano, Italy*

[6] *Technical Research Center, Indian Association for the Cultivation of Science, 2A & 2B Raja S. C. Mullick Road, Jadavpur, Kolkata 700032, India*

(Received 10 August 2021; revised 6 October 2021; accepted 18 November 2021; published 9 December 2021)

Various exotic magnetic ground states have been anticipated in the higher transition metal (4*d* and 5*d*) oxides with large atomic spin-orbit coupling (SOC). However, many such expectations were not met because the exact atomic SOC strength and its consequent influence on electronic and magnetic ground states were always masked by solid-state effects. Here, we attempt to dope a dilute amount of Ir^{5+} ($x = 0.1$–0.3) in place of Sb^{5+} in perfectly cubic Ba_2YSbO_6 with a target to minimize the effects of hopping between distant Ir ions and noncubic crystal field effect to promote the effect of SOC and to realize the coveted $J_{\text{eff}} = 0$ ground state, expected for jj-coupled $5d^4$ Ir^{5+} systems, purely from the consideration of atomic SOC. However, despite certain inhomogeneity in the distribution of the dopant Ir^{5+} ions in the system, our experimental results reveal high magnetic moments (away from the $J_{\text{eff}} = 0$ picture) with strong nearest-neighbor interaction, but without any long-range ordering, for the lowest doped system which continues to decrease with increasing Ir content, completely contrary to the expectation of the jj-coupling description. This observation strongly indicates that presence of a localized Ir moment, originating from *L*-*S* coupling interaction, might be the most appropriate mechanism here.

DOI: 10.1103/PhysRevB.104.214414

I. INTRODUCTION

Spin-orbit coupling (SOC) in correlated materials has become a subject of intensive research across many different disciplines because of its role in creating exotic classes of electronic materials. Especially when the spin, orbital, and lattice energy scales become comparable, the interplay between different degrees of freedom becomes allowed and many interesting many-body states energe, such as topological insulators [1,2], quantum spin liquids [3,4], and multipolar ordered states [5,6]. Iridates, in particular, have turned out to be a fertile ground for the complex interplay between the SOC, intra-atomic Coulomb repulsion (U), and crystal field energy (Δ_{CFE}) among others, which resulted in a diverse spectrum of exotic physical properties [7–15]. The inclusion of SOC unravelled the unexpected Mott insulating state in the layered tetravalent iridate [13] (d^5) Sr_2IrO_4, which was contrary to the conventional expectation of uncorrelated band metallicity in the system. Despite having delocalized 5*d* states, a small correlation energy U splits the narrow J_{eff} bands, appearing due to large SOC, to stabilize an insulating state. A more intriguing state is predicted in the case of d^4 pentavalent iridates where a nonmagnetic singlet $J_{\text{eff}} = 0$ ($\sum m_J = M_J = 0$) state is expected in the strong spin-orbit coupled regime [16]. However, all known d^4 systems are invariably found to show the presence of a finite magnetic moment and, consequently, a prolonged debate has been stirred up [17–22]. Among these possible d^4 systems, Ba_2YIrO_6 was the most promising one to have a pure nonmagnetic ground state because of its nearly site-ordered perfect cubic structure (space group $Fm\bar{3}m$), where each IrO_6 octahedra remains ideal, making noncubic crystal field $\Delta_{\text{CFE}}^{\text{NC}}$ to be zero [23–25]. As SOC is an atomic phenomenon, such isolated Ir^{5+} ions (Ir-Ir distance close to 6 Å) without any effect of noncubic crystal field are expected to have very strong SOC (λ). Fitting of resonant inelastic x-ray scattering data by many-body calculation of isolated Ir atoms revealed the λ to be 0.39 eV [23]. This high value of atomic λ should deny any excitonic magnetism in the system and, consequently, generation of any moment. However, contrary to expectations, Ba_2YIrO_6 showed a moment of 0.4 μ_B/f.u. [26] and an even larger moment has been found in Sr_2YIrO_6 with similar λ but significant noncubic crystal field, which only point toward the insufficiency of atomic model in these systems [27]. This deviation from the nonmagnetic $J_{\text{eff}} = 0$ ground state was ascribed to the hopping-induced delocalization of holes and intermediate state of $d^3 - d^5$ and $d^2 - d^6$, leading to the generation of magnetic moments [23].

To drastically reduce the effective hopping between the Ir^{5+} ions, we have tried to isolate Ir^{5+} ions further by doping

*mssr@iacs.res.in

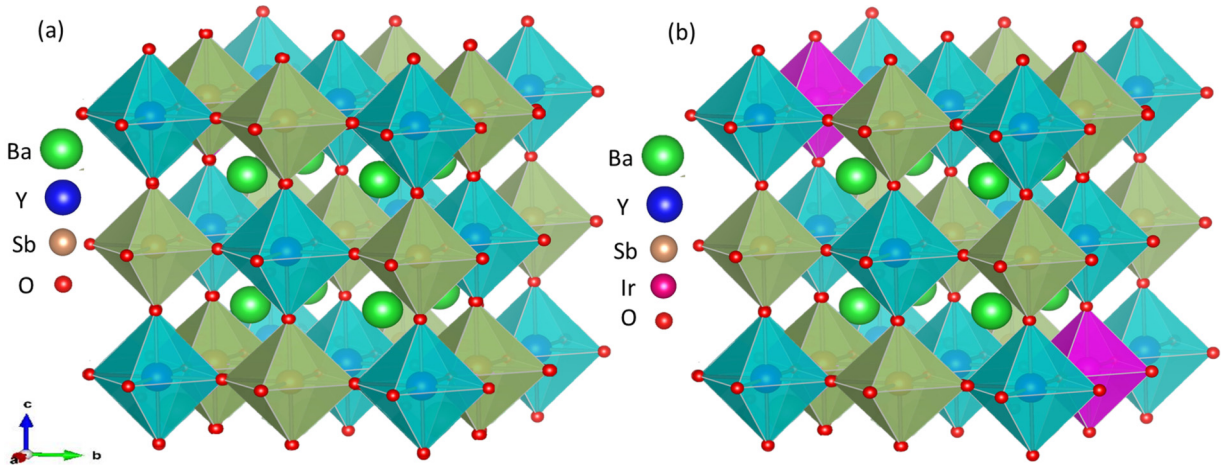

FIG. 1. Ideal crystal structure of (a) cubic Ba_2YSbO_6 and (b) Expected Ir doped $Ba_2YSb_{1-x}Ir_xO_6$ system.

them in the nonmagnetic analog Ba_2YSbO_6 in dilute amounts ($x = 0.1, 0.2, 0.3$) (Fig. 1) with a hope that the true strength of the atomic SOC could then be realized. Ba_2YSbO_6 was chosen for doping Ir as it is also a perfect cubic double perovskite without any distortion which crystalizes in the $Fm\bar{3}m$ space group with very similar lattice parameters like Ba_2YIrO_6 and, importantly, there is no magnetic ion in the host sample, which makes it a perfect choice for the investigation [28,29]. However, even though we find no evidence of any long-range magnetic ordering down to 1.4 K in these doped systems, a significant magnetic moment ($\sim$0.55–0.87 μ_B) with perceptible negative Θ_{CW} was observed (see Table II) in all the doped compounds. Our microstructural studies interestingly reveal that the dopant Ir^{5+} ions exhibit a clear preference for physical proximity, so much so that small fractions of nearly pure Ba_2YIrO_6-like phases seems to appear in all the cases. However, the major phase still remains to be the Ir-doped $Ba_2YSb_{1-x}Ir_xO_6$, albeit with reduced effective x (the rest of the Ir^{5+} ions become part of the Ba_2YIrO_6-like islands) and, therefore, our proposition could still be probed. However, the large moment of $\sim$0.87 μ_B/Ir in 10% Ir-doped system and the gradual reduction of the same with increasing Ir-doping (Table II), clearly goes contrary to the expectation of a jj-coupling picture. The decrease of the magnetic moment with increasing Ir-O bandwidth, as observed in valence band photoemission experiments, only points toward standard L-S coupled localized magnetic moment picture. The local spin dynamics probed by muon spin relaxation (μSR) also does not show any long-range magnetic ordering down to 1.4 K but indicates weak relaxation and a Gaussian nature of the internal fields due to Sb nuclear magnetism with increasing the concentration of Sb, unlike in the parent Ba_2YIrO_6.

II. SAMPLE PREPARATION, CHARACTERIZATION, AND EXPERIMENTAL DETAILS

All the samples of the $Ba_2YSb_{1-x}Ir_xO_6$ series ($x = 0.1, 0.2, 0.3$; hereafter identified as BYSIO-10, BYSIO-20, BYSIO-30) were synthesized following the conventional solid-state reaction method. Stoichiometric amounts of high purity (99.9%) starting materials of $BaCO_3$, Y_2O_3, Sb_2O_5, and IrO_2 was mixed and ground thoroughly in a mortar. Before weighing, $BaCO_3$ and Y_2O_3 were kept in an oven for more than 24 h at 150 °C to get the exact stoichiometric weight of the

TABLE I. Local structure parameters as obtained from the refinement of Ir L_3-edge EXAFS data for the three samples. The fixed or constrained values are labeled by $*$. The absolute mismatch between the experimental data and the best fit are $R^2 = 0.09$, 0.05, and 0.05 for BYSIO-10, BYSIO-20, and BYSIO-30, respectively.

Sample	Shell	(N)	σ^2 x10^{-2} (Å^2)	R(Å)
	Ir-Y	5.7	0.16	4.17(1)
	Ir-Ir(anti-site disorder)	0.3(1)	0.16$*$	4.17
BYSIO-10	Ir-Sb	9.0	0.47	6.16
	Ir-Ir	3.0(3)	0.47$*$	6.16(2)
	Ir-Y	5.5	0.12	4.20(1)
	Ir-Ir(anti-site disorder)	0.5(1)	0.12$*$	4.20
BYSIO-20	Ir-Sb	8.5	0.76	6.13
	Ir-Ir	3.5(1)	0.76$*$	6.13(4)
	Ir-Y	5.2	0.11	4.21(4)
	Ir-Ir(anti-site disorder)	0.8(1)	0.11$*$	4.21
BYSIO-30	Ir-Sb	7.0	0.83	6.19
	Ir-Ir	5.0(1)	0.83$*$	6.19(8)

TABLE II. Comparative magnetic moment of the three compounds (BYSIO-10, BYSIO-20, BYSIO-30) along with reported pure Ba_2YIrO_6 [26].

Sample	μ_{eff}	θ_{CW}
Ba_2YIrO_6	$0.44\mu_B$/Ir	~ -10 K
BYSIO-30	$0.55\mu_B$/Ir	-42 K
BYSIO-20	$0.67\mu_B$/Ir	-31 K
BYSIO-10	$0.87\mu_B$/Ir	-48 K

compounds. The mixture was then pressed into pellets and heated at 800 °C for 12 h. Finally, the pellets were annealed at 1300 °C repeatedly with intermediate grinding. Room temperature x-ray powder diffraction (XRD) pattern was collected to check the phase purity of the sample from Rigaku Smart Lab x-ray diffractometer with Cu K_α radiation. The crystal structure of this sample was obtained after refining the XRD data by Rietveld technique using FULLPROF program [30]. The x-ray photoelectron spectroscopy (XPS) measurements were carried out using an OMICRON electron spectrometer, equipped with Scienta Omicron SPHERA analyzer and Al K_α monochromatic source with an energy resolution of 0.5 eV. The surface of the pelletized sample was cleaned *in situ* by argon sputtering. The collected spectra were then processed and analyzed with the KOLXPD program. The Ir L_3 edge (∼11.2 keV) XAFS experiment at ambient temperature was performed at the XAFS beamline of Elettra synchrotron radiation facility in Italy [31]. The incident energy was set using the Si(111) double crystal monochromator where a couple of mirrors were used for efficient harmonic suppression. All the measurements were carried out in fluorescence mode with a silicon drift detector as the concentration of Ir in compounds were low. The collected EXAFS data were processed and analyzed using the freely available DEMETER package [33,34] (ATHENA and ARTEMIS). The magnetic measurements, i.e., temperature dependence of dc magnetic susceptibility (χ) and field dependence of magnetization was measured using the Quantum Design (SQUID) magnetometer. The muon spin resonance (μSR) experiment was performed using MUON spectrometer at ISIS Neutron and Muon source facility in the United Kingdom. The sample BYSIO-20 Ir L_3 edge high resolution resonant inelastic x-ray (RIXS) experiment was performed at the ID20 beamline at the ESRF synchrotron radiation facilty, Grenoble, France using π-polarized photon and a scattering geometry with $2\theta \simeq 90^\circ$ to suppress the elastic scattering [35].

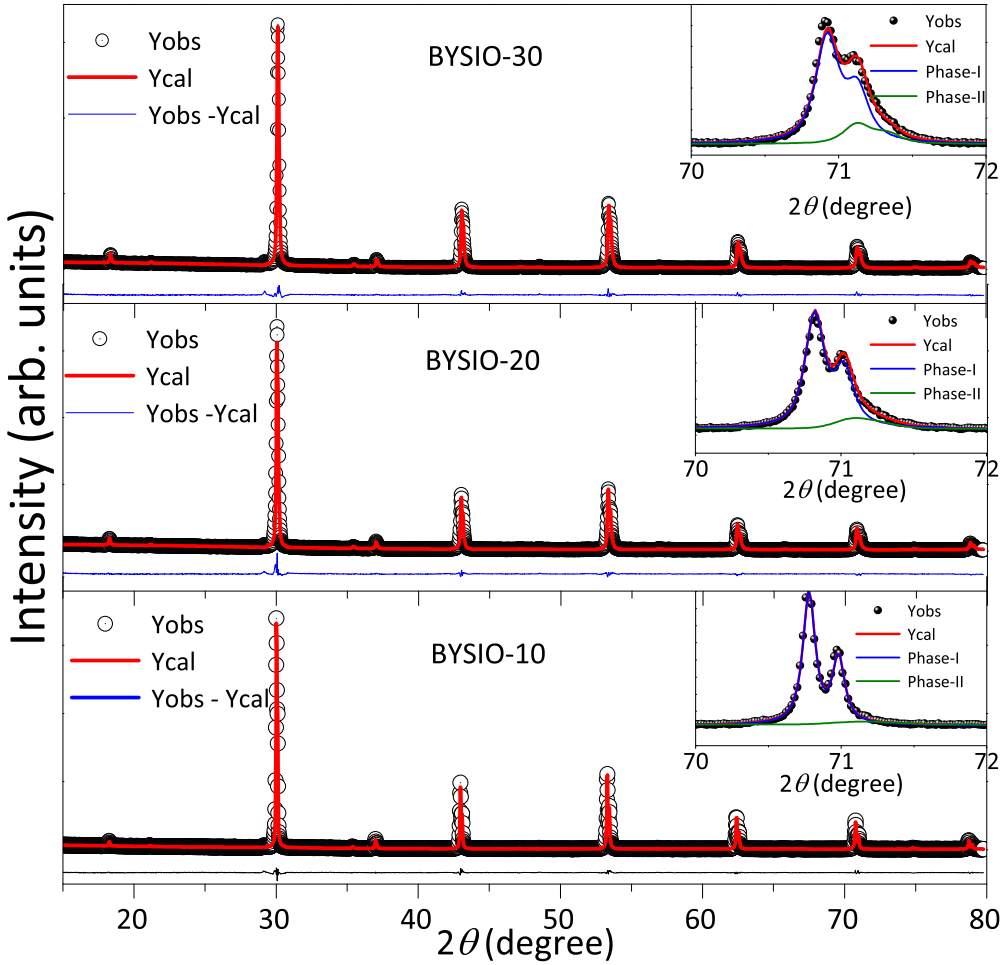

FIG. 2. Rietveld refined XRD pattern of $Ba_2YSb_{1-x}Ir_xO_6$ ($x = 0.1, 0.2, 0.3$; BYSIO-10, BYSIO-20, BYSIO-30) sample at 300 K and the top right corner inset shows the endlarged view at a higher angle of the contribution of both crystallographic phases with increased Ir doping.

III. RESULTS AND DISCUSSION

A. Crystal structure from XRD

The 300 K x-ray diffraction pattern and the best fit refined curves for all the polycrystalline $Ba_2YSb_{1-x}Ir_xO_6$ ($x = 0.1$, 0.2, 0.3) samples have been shown in Fig. 2. The structural refinement revealed two cubic phases (space group $Fm\bar{3}m$) for all the samples with different crystallographic parameters. In the inset, an expanded view of a higher angle intensity peak along with fitting phases have been shown, which reveal the change in the contribution of two crystallographic phases as a function of the doping concentration of Ir in the system. The refined lattice parameters, atomic coordinates, and site occupancies along with the goodness factors are summarized in the Supplemental Material [36]. Our analysis revealed that both phases; the dominating one with Ir-doped $Ba_2YSb_{1-x}Ir_xO_6$ (x being lesser than the intended doping concentration, phase I) as well as the small Ba_2YIrO_6 (phase II) crystalize in the cubic $Fm\bar{3}m$ space group. Single phase fitting did not yield better fitting and for the $x = 0.3$ doped sample, the fitting becomes worse. Substituting a slightly lower sized cation Ir^{5+} ($\langle r\rangle_{Ir^{5+}} = 0.57$ Å) into the Sb^{5+} ($\langle r\rangle_{Sb^{5+}} = 0.6$ Å) site causes a slight decrease in cubic lattice parameter of phase I (see Fig. 3), which is the dominant crystallographic phase, whereas the lattice parameter corresponding to Ba_2YIrO_6 (BYIO) does not vary much and remains almost constant. There is a slight indication of a certain degree of Ir/Y anti-site disorder in the BYIO phase, which apparently grows with the increase of Ir-doping concentration as can be seen in the inset to Fig. 2, but the results are not conclusive enough. Although no lattice distortion was found in any of the samples, it is important to note that the presence of a Ba_2YIrO_6 phase having certain degree of Ir/Y disorder may introduce a small amount of Ir-O-Ir hopping possibilities.

B. Local structure from EXAFS

Although an XAFS measurement cannot directly probe the phase separation in a system, it is highly sensitive to the local coordination geometry around the absorbing (Ir) atom [37,38]. Figure 4 shows the EXAFS spectra and best-fitting curves for all three samples in the fourier transformed R space, which is the radial distribution function around the Ir atom. The complexity of $Ba_2YSb_{1-x}Ir_xO_6$ structures implies many structural parameters to be refined. Reducing this number and the correlations among them is mandatory to achieve reliable results. To this aim, we applied structural constraints to the best fit parameters based on the crystallographic structures refined from XRD data. The resulting local structure around Ir in the three samples are compatible with those obtained from XRD analysis, giving confidence in the correctness of the results. The detailed fitting method and parameters are provided in the Supplemental Material [36]. The first peak at ~ 2 Å in the R-space curve corresponds to the first coordination shell around Ir (uncorrected for phase shift), i.e., the octahedral IrO_6 environment. The absence of change in intensity and width of the peak, with increasing doping, demonstrates a very similar Ir-O distribution and signifies negligible noncubic distortion around the IrO_6 octahedra consistent with our XRD analysis. The next major peak at around

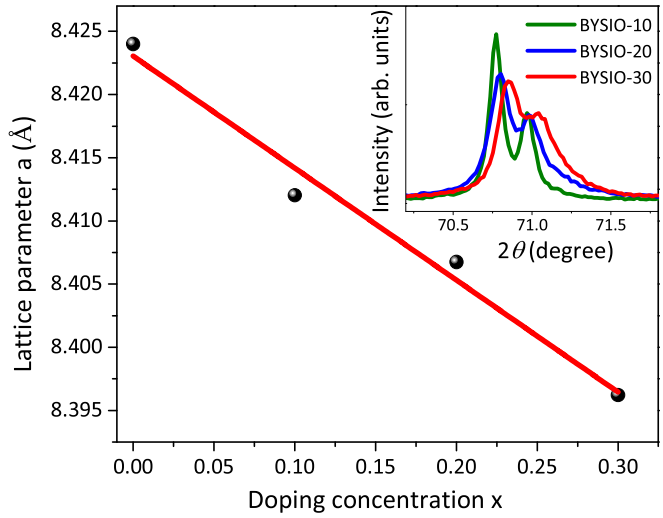

FIG. 3. Lattice parameter variation of $Ba_2YSb_{1-x}Ir_xO_6$ phase-I ($x = 0$ point has been taken from Ref. [32] for comparison); inset: shift of intensity peak at higher angle with increased doping.

3.4–4.4 Å corresponds to single and multiscattering paths from the next-neighbor atom, which gradually modifies with increasing Ir doping due to mixed contributions from single and multiple scattering paths from Ir and Y next-neighbors. Evidently, this indicates next-neighbor contributions, being roughly in the antiphase (see Fig. S1). Our EXAFS analysis is consistent with XRD analysis showing $N_{Ir-Y} = 5.7$, 5.5, and 5.2 for $x = 0.1$–0.3 instead of 6 as expected for a completely ordered arrangement, signifying increase in anti-site disorder between Ir and Y with doping (from 5% in $x = 0.1$ to 13% in $x = 0.3$), which is in agreement with our XRD analysis (see Table I). Further, to understand the distribution of dopant Ir substituting Sb, the feature around ~ 6 Å was analyzed. In an ideal homogeneous distribution of Ir in the system, the central Ir should see 1.2 (10.8), 2.4 (9.6), and 3.6 (8.4) N_{Ir-Ir} ($N_{Ir\text{-}Sb}$) neighbors for $x = 0.1$, 0.2, and 0.3, respectively. However, our analysis yielded $N_{Ir\text{-}Ir}$ ($N_{Ir\text{-}Sb}$) to be systematically larger (smaller) being 3.0 (9.0), 3.5 (8.5), and 5.0 (7.0), indicating slightly preferred Ir over Sb at around 6 Å. This effect is weak, however, can be taken as indicative of not perfectly homogeneous distribution of Ir in the system, leading to some phase separation. Such inhomogeneity would likely influence the magnetic ground state of these systems.

C. Ir oxidation state from XPS

It is important to know the charge state of the magnetic ion in the sample as the origin of the magnetic moment could be greatly affected by the presence of Ir^{4+} or Ir^{6+} ions [13,39–41]. X-ray photoelectron spectra of Ir $4f$ core shell were collected and fitted with a spin-orbit doublet shown in the inset of Figs. 5(a)–5(c). The energy positions of $4f_{7/2}$ (63.14 eV, 63.13 eV, and 63.35 eV) and $4f_{5/2}$ (66.19 eV, 66.19 eV, and 66.40 eV) doublets of the corresponding compounds BYSIO-10, BYSIO-20, and BYSIO-30, along with their spin-orbit separation around 3.05 eV, 3.04 eV, and 3.05 eV ensured the sole presence of Ir^{5+} ions in all the samples and no trace of any other magnetic ion was found. The valence band spectra

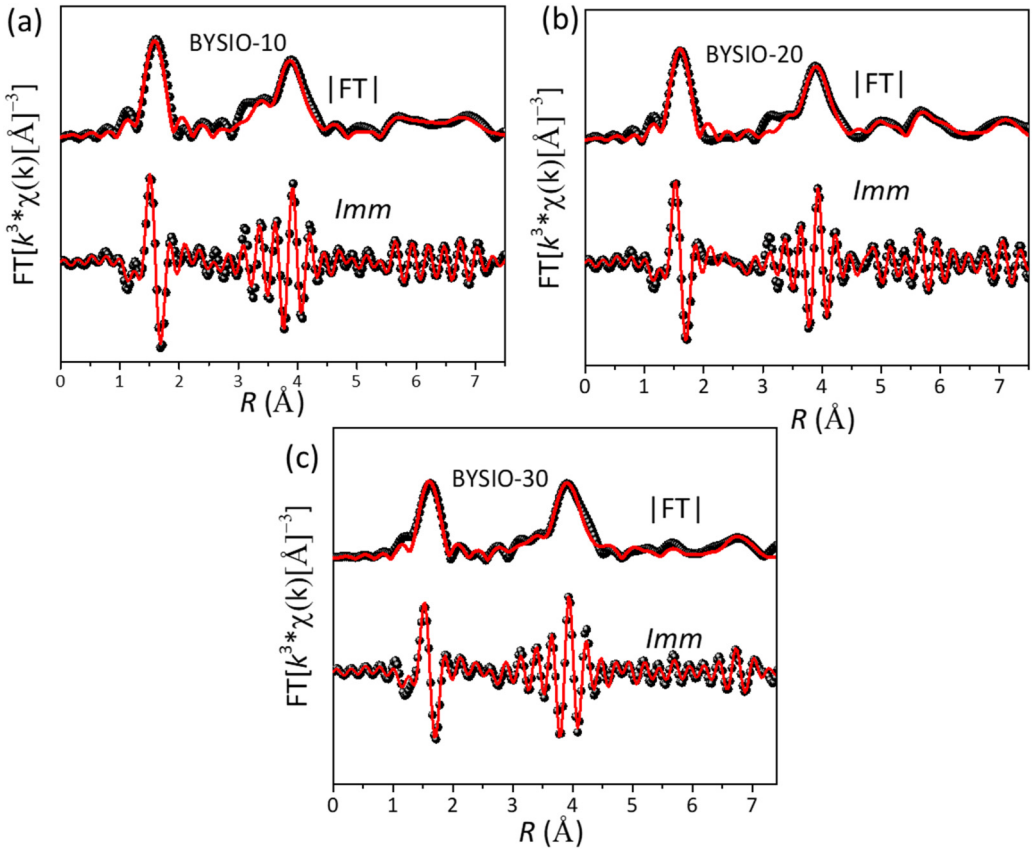

FIG. 4. The Fourier transforms of the Ir L_3-edge k^3 weighted EXAFS experimental data; magnitude (FT), imaginary part (*Imm*), and the fitted curves of (a) BYSIO-10, (b) BYSIO-20, and (c) BYSIO-30 samples.

of all three compounds are shown in the main window of Figs. 5(a)–5(c) with no density of states at the Fermi level affirming the insulating nature of all the compounds, consistent with the electronic behavior of Ba_2YIrO_6 as well as with Ba_2YSbO_6, which is a highly insulating dielectric material [28,29]. However, near the Fermi level (E_F), a peaklike feature intensifies with the increased concentration of Ir in the system. The density of states near E_F is expected to be contributed by Ir-O hybridized bands, which continues to grow with increasing Ir doping. This finding comes in agreement with the fact that with increasing Ir-doping the Ir-O hybridized band should gain in intensity, which is clearly the case here. However, it should be noted that such a situation is obviously detrimental to realizing atomic SOC as well as the coveted $J_{\text{eff}} = 0$ nonmagnetic ground state in the system and, therefore, one would expect progressive departure from the $J_{\text{eff}} = 0$ nonmagnetic ground state and increase in magnetic moment with doping.

D. Magnetic susceptibility

Temperature-dependent bulk dc magnetic susceptibility for all the samples have been measured and shown in Figs. 6(a)–6(c). Zero-field cooled (ZFC) and field-cooled (FC) data were

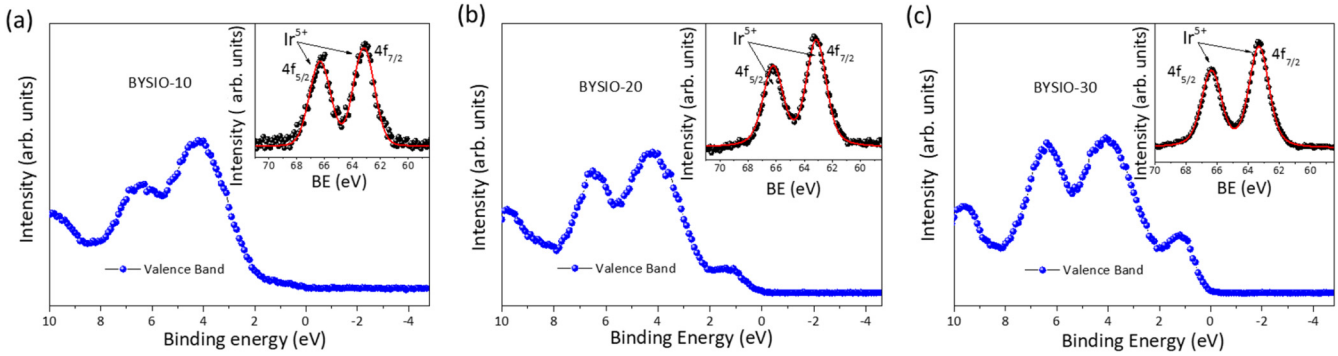

FIG. 5. XPS Valence band spectra of (a) BYSIO-10, (b) BYSIO-20, and (c) BYSIO-30 sample at 300 K and in the inset the corresponding Ir $4f$ core level spectra (black sphere) and the corresponding fitting (red solid line).

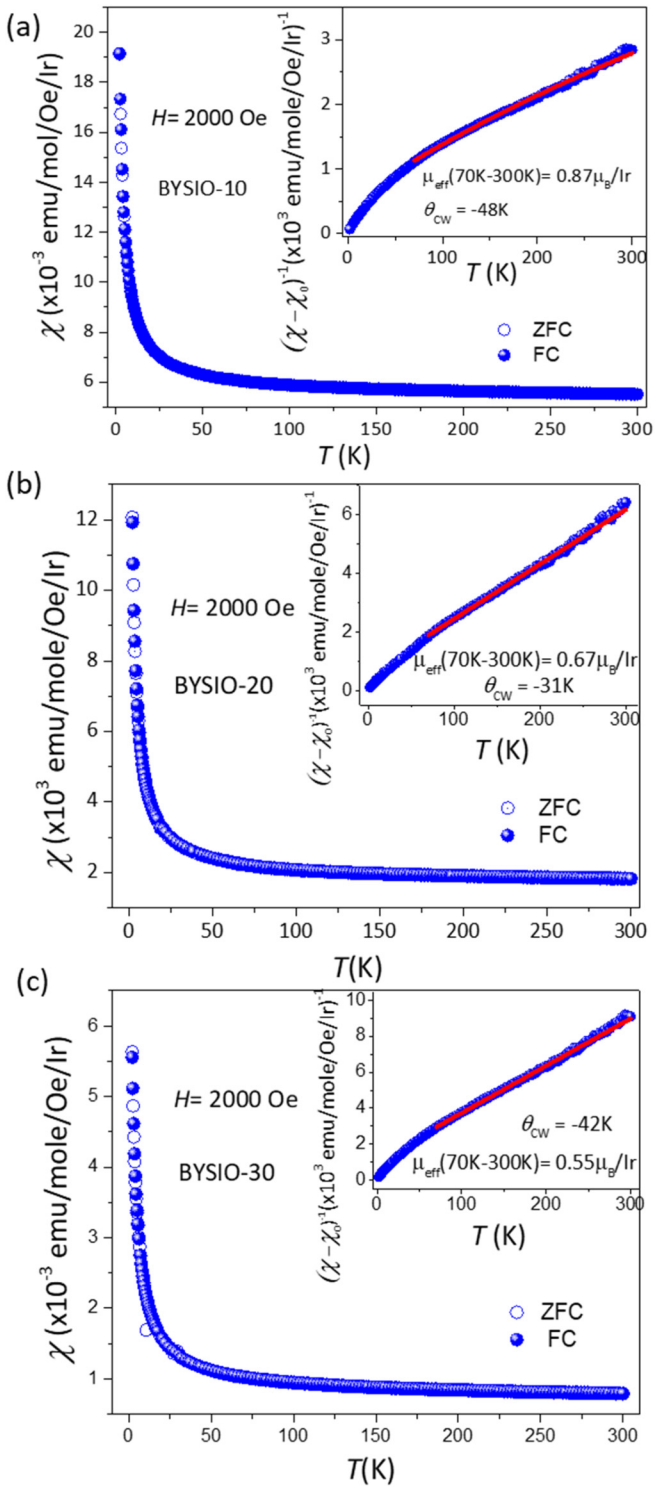

FIG. 6. Temperature-dependent dc susceptibility variations during zero-field-cooled (open blue circles) and field-cooled (shaded blue circles) plotted for (a) BYSIO-10, (b) BYSIO-20, and (c) BYSIO-30 ($x = 0.1, 0.2, 0.3$) samples. Inset: Temperature dependence of $1/(\chi\text{-}\chi_0)$ is plotted with Curie-Weiss fitting (red solid line).

recorded in the temperature range of 2 K to 300 K in the applied filed of 2000 Oe. The inset to Figs. 6(a)–6(c) shows inverse magnetic susceptibility $(1/\chi)$ where the solid red lines indicate linear dependence in the range of 70 K $< T <$ 300 K. The linear fit was carried out using the Curie-Weiss (CW) equation $\chi = \frac{C}{T-\Theta_{CW}} + \chi_0$, where C is the Curie constant while Θ_{CW} and χ_0 represent the CW temperature and the temperature-independent susceptibility, respectively. It is worth mentioning that absence of any long-range magnetic ordering down to at least 2 K and deviation of CW fits below 70 K in all samples with strong negative Θ_{CW} clearly suggest that these systems are not simple paramagnets as the frustration parameters are high, reminiscent of quantum spin-liquid systems [42,43]. Most interestingly, the CW fitting yields effective magnetic moments of 0.87 μ_B/Ir, 0.66 μ_B/Ir, and 0.55 μ_B/Ir for BYSIO-10, BYSIO-20, and BYSIO-30, respectively, which immediately contradict the expectations of jj-coupling description, as described above. The corresponding Θ_{CW} varies between -45 K to -30 K, considering the uncertainties (see Table II), which point toward antiferromagnetic interactions between neighboring Ir^{5+} ions in all three samples.

This large effective magnetic moment and high value of negative Θ_{CW} in Ir-diluted samples may seem unreasonable because of the anticipation of weak interaction between Ir^{5+} ions, which are expected to be largely separated within the lattice. Even though the observed inhomogeneous distribution of dopant Ir may enforce a certain degree of enhanced hopping connectivity weakening the SOC, it should be noted that even then the closest Ir-Ir distance that can be achieved in the system is above 6 Å similar to Ba_2YIrO_6 where the observed magnetic moment hovers around 0.4 μ_B/Ir only and, therefore, a moment of 0.87 μ_B/Ir for BYSIO-10 seems unexplainable. Additionally, increasing Ir doping only ensures increased Ir-O bandwidth with doping, which is expected to have a detrimental effect on SOC (λ) and, consequently, the system is expected to shift away further from the atomic $J_{\text{eff}} = 0$ situation progressively, i.e., moments are only expected to increase with x. Therefore, the observed opposite trend in the moment creates a serious doubt on the assumption of jj coupling in the system, as has been mentioned in cases of other iridates recently [44].

E. Resonant inelastic x-ray scattering

Elementary excitations probed by resonant inelastic x-ray scattering (RIXS) have strengthened our understanding of complex magnetic ground states and established the role of SOC in iridates [45–48]. There have been several attempts to quantify the value of SOC by modeling the RIXS features with single-atom full-multiplet calculations. However, we did show earlier that the simple approach of identifying all these RIXS features directly with purely atomic excitations can be rather erroneous in the context of extended solids [27], where hopping and other solid-state effects do play the role of the spoiler. Here, we carry out the high- and low-resolution RIXS experiments at 20 K (only high resolution) and 300 K on one of the doped compounds BYSIO-20 with a fixed photon incident energy at 11216 eV and compare them with the same from Ba_2YIrO_6. The details of the low-resolution, high-energy features have been discussed in the Supplemental Material [36], while low-energy excitations are shown in Fig. 7. Even though extracting the atomic SOC value directly from the energy positions of these RIXS features may not

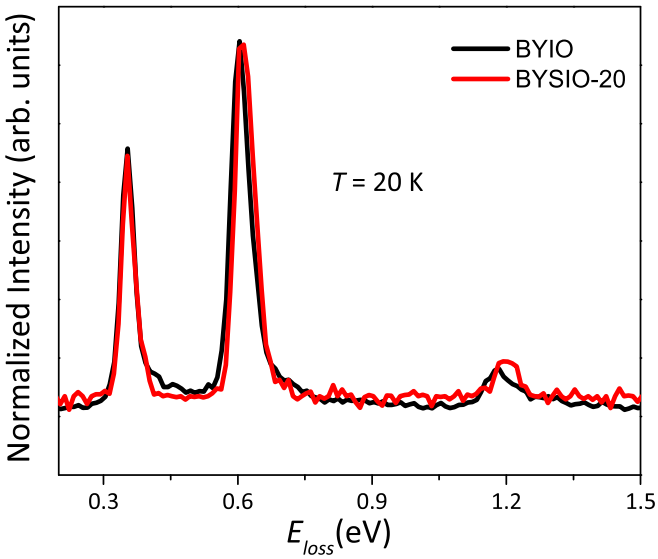

FIG. 7. Normalized high-resolution low energy RIXS spectra at $T = 20$ K of the samples BYSIO-20 (solid red line) and Ba_2YIrO_6 (solid black line) for comparison.

be truly meaningful, the comparison indicates small shifts in these low-energy excitations toward higher energies which in turn are indicative of slightly enhanced SOC in BYSIO-20 compared to BYIO. Once again, this effect only proves that increasing SOC isn't decreasing moments and, therefore, is difficult to describe within the realm of jj coupling.

F. Muon spin relaxation-μSR

μSR is an outstanding tool to probe spin order and dynamics of any magnetic ion in a material at the local level. Zero-field muon spin relaxation (μSR) has been performed on the most diluted BYSIO-10 and BYSIO-20 samples to get insight into the magnetic nature of these Ir-diluted double perovskite systems (see Fig. 8). No oscillations were observed in any of the samples down to 1.4 K, confirming the absence of long-range magnetic order in these compounds, consistent with magnetic susceptibility data [Figs. 8(a) and 8(b)]. The muon relaxation behavior of the compounds as the concentration of Ir is diluted tends to differ significantly from Ba_2YIrO_6. While the relaxation nature of the latter could be well explained by simple stretched exponential $e^{(-\lambda' t)^{\beta}}$, such fitting largely fails for BYSIO-20 ($x = 0.2$) and could not fit the BYSIO-10 at all.

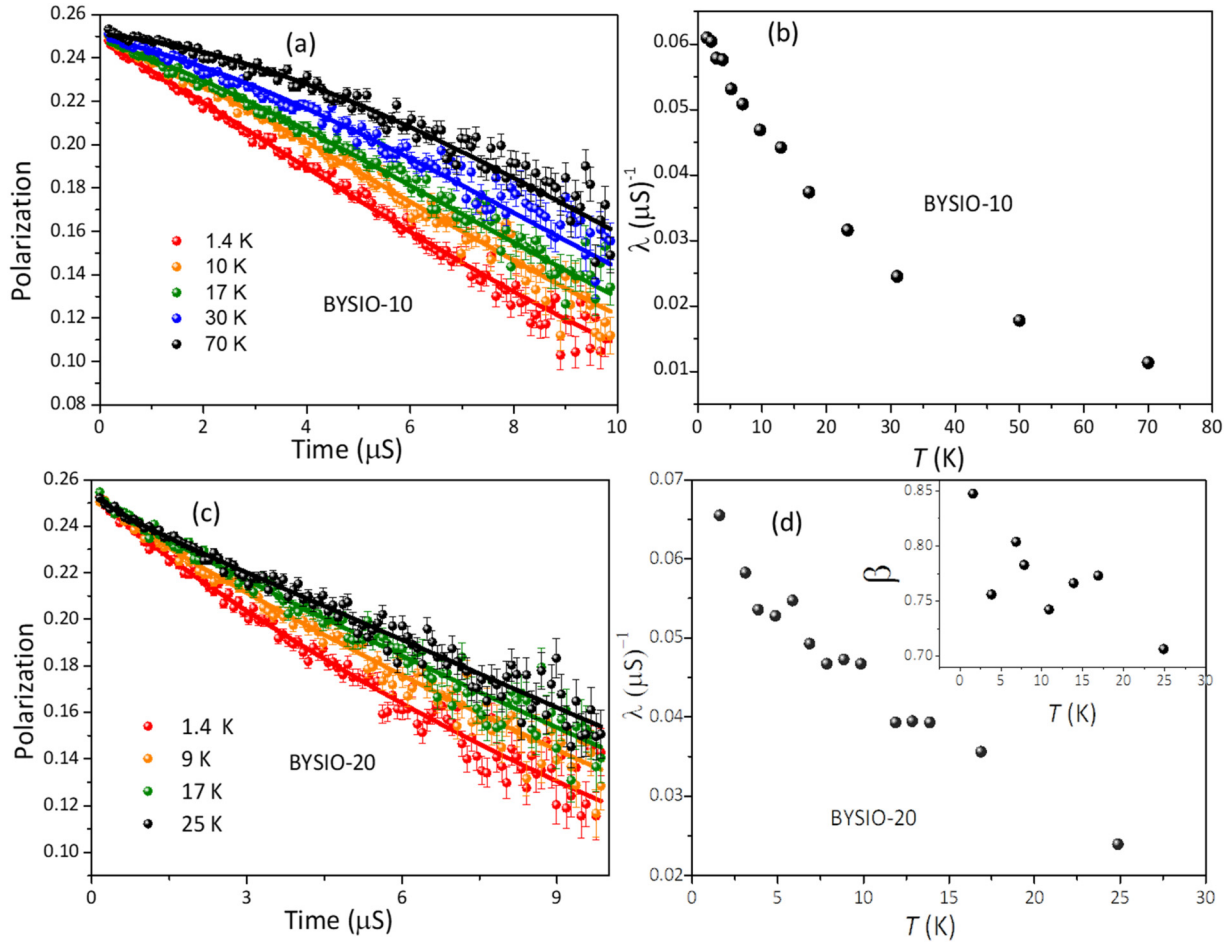

FIG. 8. Time evolution of muon polarization in zero external field at different temperature for (a) BYSIO-10 ($x = 0.1$) (c) BYSIO-20 ($x = 0.2$) samples and the corresponding relaxation rate also indicated in (b) and (d), inset; temperature evolution of β.

Considering the stronger Gaussian nature of muon spin relaxation in the diluted compounds, we have fitted the BYSIO-10 data with the following function:

$$P(t) \sim A_0 + A_1 G^{\mathrm{KT}}(t, \Delta) e^{(-\lambda' t)^{\beta}}, \quad (1)$$

where $G^{\mathrm{KT}}(t, \Delta)$, the static Gaussian Kubo-Toyabe function corresponding to a field distribution width Δ, is multiplied by the exponential $e^{(-\lambda' t)^{\beta}}$. The Kubo-Toyabe component naturally arises from Sb nuclear magnetism. The weak nuclear dipolar field of Sb (I=5/2) can be considered static in the μSR time window. The internal local Gaussian field strength $\frac{\Delta}{\gamma}$ for BYSIO-10 is 0.076 mT, which is a little higher than 0.06 mT for BYSIO-20. In addition, the diluted Ir^{5+} ions in the system keep fluctuating, likely due to inhomogenity and spatial disorder creating geometrical frustration, which is described by the stretched exponential component of Eq. (1). The muon spin relaxation for both samples keeps increasing at lower temperatures down to 1.4 K. At the lowest measured temperature value of 1.4 K, the relaxation rate of $\lambda'_{\mathrm{BYSIO-20}}$ is $\sim$ 0.066 μS^{-1}, which is similar to $\lambda'_{\mathrm{BYSIO-10}}$ $\sim$ 0.061 μS^{-1}. For BYSIO-10, β could be fixed to 1 (pure exponential dynamical relaxation) while the deviation of β from 1 in BYSIO-20 [inset of Fig. 8(d)] to lower values with increasing temperature evidently points toward more inhomogeneous distribution [49,50] of Ir^{5+} ions with increasing concentration of Ir, which is in accordance with the EXAFS and x-ray diffraction refinement analysis.

IV. CONCLUSION

In summary, we conclude that the attempt to dilute dope Ba_2YSbO_6 with Ir yields a somewhat inhomogeneous distribution of the dopant ion in the system, giving rise to formation of minor BYIO-like clusters within the dominant phase of BYSIO having somewhat less than nominal Ir content. While increasing Ir content does increase the Ir-O bandwidth, the magnetic moment surprisingly decreases progressively. RIXS measurements do indicate a slight increase in SOC for systems with lesser Ir content, but the simultaneous increase of Ir moments puts the jj-coupling description in question. Muon spin relaxation study confirmed no unambiguous sign of magnetic ordering down to 1.4 K and Gaussian nature of local internal magnetic field was observed due to weak dipolar Sb nuclear interaction along with the fluctuating nature of Ir^{5+} spins down to 1.4 K.

ACKNOWLEDGMENTS

M.S.K. thanks UGC India and IACS for fellowship. S.R. thanks Technical Research Center (TRC) of IACS for providing experimental facilities. Authors also thank Prof. Subham Majumdar of IACS for useful discussions. S.R. also thanks SERB, DST for financial support (Project No. CRG/2019/003522).

[1] W. Witczak-Krempa, G. Chen, Y. B. Kim, and L. Balents, Annu. Rev. Condens. Matter Phys. **5**, 57 (2014).
[2] X. Wan, A. M. Turner, A. Vishwanath, and S. Y. Savrasov, Phys. Rev. B **83**, 205101 (2011).
[3] L.T. Corredor, G. Aslan-Cansever, M. Sturza, K. Manna, A. Maljuk, S. Gass, T. Dey, A.U.B. Wolter, O. Kataeva, A. Zimmermann, M. Geyer, C. G. F. Blum, S. Wurmehl, and B. Buchner, Phys. Rev. B **95**, 064418 (2017).
[4] A. Nag, S. Middey, S. Bhowal, S. K. Panda, R. Mathieu, J. C. Orain, F. Bert, P. Mendels, P. G. Freeman, M. Mansson, H. M. Ronnow, M. Telling, P. K. Biswas, D. Sheptyakov, S. D. Kaushik, V. Siruguri, C. Meneghini, D. D. Sarma, I. Dasgupta, and S. Ray, Phys. Rev. Lett. **116**, 097205 (2016).
[5] G. Chen and L. Balents, Phys. Rev. B **84**, 094420 (2011).
[6] G. Chen, R. Pereira, and L. Balents, Phys. Rev. B **82**, 174440 (2010).
[7] G. Chen and L. Balents, Phys. Rev. B **78**, 094403 (2008).
[8] M. J. Lawler, A. Paramekanti, Y. B. Kim, and L. Balents, Phys. Rev. Lett. **101**, 197202 (2008).
[9] D. Pesin and L. Balents, Nat. Phys. **6**, 376 (2010).
[10] K. Matsuhira, M. Wakeshima, R. Nakanishi, T. Yamada, A. Nakamura, W. Kawano, S. Takagi, and Y. Hinatsu, J. Phys. Soc. Jpn. **76**, 043706 (2007).
[11] H. Fukazawa and Y. Maeno, J. Phys. Soc. Jpn. **71**, 2578 (2002).
[12] S. Nakatsuji, Y. Machida, Y. Maeno, T. Tayama, T. Sakakibara, J. van Duijn, L. Balicas, J. N. Millican, R. T. Macaluso, and J. Y. Chan, Phys. Rev. Lett. **96**, 087204 (2006).
[13] B. J. Kim, H. Jin, S. J. Moon, J. Y. Kim, B. G. Park, C. S. Leem, J. Yu, T. W. Noh, C. Kim, S. J. Oh, J. H. Park, V. Durairaj, G. Cao, and E. Rotenberg, Phys. Rev. Lett. **101**, 076402 (2008).
[14] S. J. Moon, H. Jin, K. W. Kim, W. S. Choi, Y. S. Lee, J. Yu, G. Cao, A. Sumi, H. Funakubo, C. Bernhard, and T. W. Noh, Phys. Rev. Lett. **101**, 226402 (2008).
[15] B. J. Kim, H. Ohsumi, T. Komesu, S. Sakai, T. Morita, H. Takagi, and T. Arima, Science **323**, 1329 (2009).
[16] G. Khaliullin, Phys. Rev. Lett. **111**, 197201 (2013).
[17] G. Cao, T. F. Qi, L. Li, J. Terzic, S. J. Yuan, L. E. DeLong, G. Murthy, and R. K. Kaul, Phys. Rev. Lett. **112**, 056402 (2014).
[18] J. Terzic, H. Zheng, F. Ye, H. D. Zhao, P. Schlottmann, L. E. De Long, S. J. Yuan, and G. Cao, Phys. Rev. B **96**, 064436 (2017).
[19] B. Ranjbar, E. Reynolds, P. Kayser, B. J. Kennedy, J. R. Hester, and J. A. Kimpton, Inorg. Chem. **54**, 10468 (2015).
[20] B. F. Phelan, E. M. Seibel, D. Badoe, Jr., W. Xie, and R. Cava, Solid State Commun. **236**, 37 (2016).
[21] M. Wakeshima, D. Harada, and Y. Hinatsu, J. Alloys Compd. **287**, 130 (1999).
[22] O. N. Meetei, W. S. Cole, M. Randeria, and N. Trivedi, Phys. Rev. B **91**, 054412 (2015).
[23] A. Nag, S. Bhowal, A. Chakraborty, M. M. Sala, A. Efimenko, F. Bert, P. K. Biswas, A. D. Hillier, M. Itoh, S. D. Kaushik, V. Siruguri, C. Meneghini, I. Dasgupta, and Sugata Ray, Phys. Rev. B. **98**, 014431 (2018).
[24] G. Chen, L. Balents, and A. P. Schnyder, Phys. Rev. Lett. **102**, 096406 (2009).

[25] T. Dodds, T. P. Choy, and Y. B. Kim, Phys. Rev. B **84**, 104439 (2011).
[26] T. Dey, A. Maljuk, D. V. Efremov, O. Kataeva, S. Gass, C. G. F. Blum, F. Steckel, D. Gruner, T. Ritschel, A. U. B. Wolter, J. Geck, C. Hess, K. Koepernik, J. van den Brink, S. Wurmehl, and B. Büchner, Phys. Rev. B. **93**, 014434 (2016).
[27] A. Nag, S. Bhowal, M. M. Sala, A. Efimenko, I. Dasgupta, and S. Ray, Phys. Rev. Lett. **123**, 017201 (2019).
[28] L. Wu, X. Mei, and W. Zheng, Mater. Lett. **60**, 2326 (2006).
[29] J. Konopka, R. Jose and M. Woácyrz, Physica C **435**, 53 (2006).
[30] J. Rodriguez Carvajal, Phys. B: Condens. Matter **192**, 55 (1993).
[31] A. Di Cicco, G. Aquilanti, M. Minicucci, E. Principi, N. Novello, A. Cognigni, and L. Olivi, J. Phys.: Conf. Ser. **190**, 012043 (2009).
[32] J. A. Alonso, C. Cascales, P. García Casado, and I. Rasines, J. Solid State Chem. **128**, 247 (1997).
[33] M. Newville, J. Synchrotron Radiat. **8**, 322 (2001).
[34] B. Ravel and M. Newville, ATHENA, ARTEMIS, HEPHAESTUS: Data analysis for X-ray absorption spectroscopy using IFEFFIT, J. Synchrotron Radiat. **12**, 537 (2005).
[35] M. M. Sala, C. Henriquet, L. Simonelli, R. Verbeni, and G. Monaco, J. Electron Spectrosc. Relat. Phenom. **188**, 150 (2013); M. M. Sala, K. Martel, C. Henriquet, A. Al Zein, L. Simonelli, C. Sahle, H. Gonzalez, M.-C. Lagier, C. Ponchut, S. Huotari, R. Verbeni, M. Krisch, and G. Monaco, J. Synchrotron Rad. **25**, 580 (2018)
[36] See Supplemental Material at http://link.aps.org/supplemental/10.1103/PhysRevB.104.214414 for detailed XRD and EXAFS refined parameters, and which includes Refs. [51–53].
[37] A. Di Cicco and A. Filipponi, J. Non-Crystalline Solids **205-207**, 304 (1996).
[38] A. Filipponi, J. Phys.: Condens. Matter **13**, R23 (2001).
[39] G. Cao, V. Durairaj, S. Chikara, L. E. DeLong, S. Parkin, and P. Schlottmann, Phys. Rev. B **76**, 100402(R) (2007).
[40] P. Kayser, M. Jesús Martínez-Lope, J. A. Alonso, M. Retuerto, M. Croft, A. Ignatov, and M. T. Fernández-Díaz, Eur. J. Inorg. Chem. **2014**, 178 (2013).
[41] G. Cao, A. Subedi, S. Calder, J.-Q. Yan, J. Yi, Z. Gai, L. Poudel, D. J. Singh, M. D. Lumsden, A. D. Christianson, B. C. Sales, and D. Mandrus, Phys. Rev. B **87**, 155136 (2013).
[42] Y. Okamoto, M. Nohara, H. Aruga-Katori, and H. Takagi, Phys. Rev. Lett. **99**, 137207 (2007).
[43] T. Dey, A. V. Mahajan, P. Khuntia, M. Baenitz, B. Koteswararao, and F. C. Chou, Phys. Rev. B **86**, 140405(R) (2012)
[44] A. Bandyopadhyay, A. Chakraborty, S. Bhowal, V. Kumar, M. M. Sala, A. Efimenko, F. Bert, P. K. Biswas, C. Meneghini, N. Büttgen, I. Dasgupta, T. Saha Dasgupta, A. V. Mahajan, and S. Ray, arXiv:2107.04431.
[45] L. J. P. Ament, G. Khaliullin, and J. van den Brink, Phys. Rev. B **84**, 020403(R) (2011).
[46] M. M. Sala, K. Ohgushi, A. Al-Zein, Y. Hirata, G. Monaco, and M. Krisch, Phys. Rev. Lett. **112**, 176402 (2014).
[47] A. Paramekanti, D. J. Singh, B. Yuan, D. Casa, A. Said, Y. J. Kim, and A. D. Christianson, Phys. Rev. B **97**, 235119 (2018).
[48] B. J. Kim and G. Khaliullin, Phys. Rev. B **96**, 085108 (2017).
[49] Y. J. Uemura, T. Yamazaki, D. R. Harshman, M. Senba, and E. J. Ansaldo, Phys. Rev. B **31**, 546 (1985).
[50] N. Gauthier, B. Prévost, A. Amato, C. Baines, V. Pomjakushin, A. D. Bianchi, R. J. Cava, and M. Kenzelmann, J. Phys.: Conf. Ser. **828**, 012014 (2017).
[51] T.Chakraborty, C. Meneghini, A. Nag, and S. Ray, J. Mater. Chem. C **3**, 8127 (2015).
[52] S. Middey, Payel Aich, C. Meneghini, K. Mukherjee, E. V. Sampathkumaran, V. Siruguri, P. Mahadevan, and Sugata Ray, Phys. Rev. B **94**, 184424 (2016).
[53] K. Ishii, I. Jarrige, M. Yoshida, K. Ikeuchi, J. Mizuki, K. Ohashi, T. Takayama, J. Matsuno, and H. Takagi, Phys. Rev. B **83**, 115121 (2011).